



Schlumberger-Doll
Research Limited,
One Hampshire Street,
MD-B253,
Cambridge,
MA 02139 USA.

Schlumberger Cambridge
Research Limited,
High Cross, Madingley Road,
Cambridge,
CB3 0EL England.
44 1223 315576

Schlumberger Moscow Research
9 Taganskaya Ulitsa,
109004 Moscow,
Russia
7 095 937 9511

Schlumberger Dhahran Carbonate Research,
Petroleum Center,
P.O. Box 2836,
Al-Khobar 31952,
Saudi Arabia
966 3 860 1710 1716

CONFIDENTIAL

OFSR/DN/2010/054/OTHER/C

**MODELING OF MULTICOMPONENT NON-ISOTHERMAL
FILTRATION IN A NEAR- WELLBORE ZONE**

Alexandra Zhabkina,, Artyom Myasnikov

Modeling of multicomponent non-isothermal filtration in a near-wellbore zone

A Department Note

Alexandra Zhabkina (MIPT, Moscow, Russia),

Artyom Myasnikov (Schlumberger Moscow Research, Reservoir Testing)

Abstract

We present in this report newly developed version of general purpose research code for modeling of thermal compositional flows in near-well bore zones. We implemented both general thermal flash and a performed beforehand phase approximating procedure in the hydrodynamical solver. The last one, previously available for isothermal case only, was extended on the thermal case. For the case of the K -values independent on phase composition, the code was validated versus E300. Some preliminary results the modeling of condensate bank recovery are presented.

Introduction

The present study is devoted to modeling of two phase multi component filtration in a near wellbore zone with taking into account various thermal effects. Although one can use some commercial software for doing that, we considered its worth to develop our own research code with proper functionalities, especially since such code has been already under development in SMR [Belov et al], [Levkovich et al], [Lysov et al].

The reason we need the specially developed code for the mentioned research activity is that, firstly, the flow in near wellbore zone strongly differs from one on reservoir large scales where conventional commercial codes like E300 are recognized as good enough. Secondly, even in the range of its applicability E300 does not allow to run thermal compositional simulations in general form since the thermal option there is restricted by the assumption that equilibrium constants do not depend on mixture composition, which is quit strong. Finally, the approximation of phase equilibrium at the preprocessing stage which we develop in the thesis may make it possibly to work directly with field PVT data if needed. So, the main objective of the present study is to develop a thermal compositional option based either on direct flash simulations or on preprocessing phase approximation, implement it in the SMR research code and validate it against E300 in the range of the later's applicability. Additionally, as long as the code is ready for applications its worth to study how the Joule-Thomson effect and adiabatic heating could influence on the steady state and transient gas condensate flows in wellbore area, since both pressure and temperature due pressure changes may lead to changing the saturation of gas/ gas condensate mixture which could affect the efficiency of condensate recovery.

In this work an extending of phase equilibrium approximation technique on non-isothermal case is realized as well. Software PVTi gives parameters of mixture under consideration. These parameters are used for phase properties calculations of the mixture. Using of approximations of

phase equilibrium on preprocessing stage makes it possible to reduce calculation time, without calling external flash library during calculation process.

1. Problem Statement

Here are the governing equations for 2-phase compositional non-isothermal filtration. It has a conventional form of mass and energy conservation laws completed by the Darcy law:

$$\frac{\partial}{\partial t}(\phi b C^k) + \nabla \cdot \left(\sum_{\alpha=1}^{N_p} C_{\alpha}^k b_{\alpha} \mathbf{w}_{\alpha} \right) = 0 \quad \alpha = L, G \quad k = 1, \dots, N_c \quad (1)$$

$$\frac{\partial E}{\partial t} + \nabla \cdot \sum_{\alpha} b_{\alpha} H_{\alpha} \mathbf{w}_{\alpha} = 0 \quad (2)$$

Where $N_p = 2$ the number of phases, $\alpha = L, G$ is the phase identifier (liquid/oil or gas); N_c - number of components; b_{α} - molar density of the phase; and the total molar density is introduced by

$$b = \sum_{\alpha=1}^{N_p} b_{\alpha} s_{\alpha}.$$

In the equation (2) the total energy is calculated as

$$E = \phi \sum_{\alpha} (b_{\alpha} H_{\alpha} - p_{\alpha}) s_{\alpha} + (1 - \phi) \rho_s U_s, \quad (3)$$

where $\rho_s U_s = H_{CR}(T - T_{st})$, ρ_s - rock density, H_{CR} - rock heat capacity (keyword HEATCR for Eclipse). Specification of phase enthalpies in (3) is chosen in the form compatible with one of the implemented in Eclipse:

$$H_L(T) = \sum_k C_L^k \mu^k H_L^k(T) \quad (4)$$

$$H_G(P, T) = \sum_k C_G^k (\mu^k H_G^k(T) + H_{JT}(P)) \quad (5)$$

That is the enthalpies of the oil and gas phases are calculated using a mole fraction weighted average of the component enthalpies. The component enthalpies, are, in turn defined in accordance with one of E300 models:

$$\begin{aligned} H_G^k(T) &= h_{O,1}^k(T - T_{st}) \\ H_G^k(T) &= H_0^k + h_{G,1}^k(T - T_{st}) \end{aligned} \quad (6)$$

Where $h_{L,1}^k$ and $h_{G,1}^k$ - oil and gas component specific heat, specified in Eclipse by keywords SPECHA и SPECHG, H_0^k - heat of vaporization at standard temperature, E300 keyword is

HEATVAPS. The pressure-dependent Joule-Thomson term $H_{JT}^k(P)$ is specified, again, as in E300:

$$H_{JT}^k = -Z_1^k \cdot (P - P_{st}) \quad (7)$$

In E300, Z_1^k is specified by keyword ZFACT1. This is a simplified model: in fact, the coefficient Z_1^k does not depend on phase composition as it should. It's connected with traditional Joule-Thomson Z_i^k coefficient as

$$Z_i^k \bar{\mu} \bar{h} = Z_1^c \quad (8)$$

where $\bar{\mu}$ and \bar{h} are average molecular weight and heat capacity of the gas phase.

2. Computational Model

The algorithm implemented in the thermal compositional research code consists of the following iterative steps. First, the derivative of overall molar density $\Delta b \equiv \partial \phi b / \partial t$ over time is treated as a finite difference unknown corrected during iterations on each time step. Its value at the first iteration is taken from the previous time step. Consider Δb is known at the n time step, as well as the primitive variables P , T , C^k and phase compositions C_α^k , densities b_α and viscosities μ_α . Then, pressure distribution is obtained by implicit solution of the Poisson equation came from summation of equations (1), substituting Darcy Law expression instead of w_α there (capillary pressures and gravity are neglected in this study). The concentrations and temperatures are updated then with newly obtained pressure field by explicit upwind scheme (in the present study we considered only the first order approximation scheme). The values of nonlinear coefficients in all equations are taken as an arithmetic average between first and current iterations.

After the new values of concentrations, pressure and temperature are obtained, the phase equilibrium problem is solved either by calling for E300 flash procedure, or by restoring the data from specially prepared at the preprocessing stage repository.

The energy equation (3) was modified in the way presented in Figure 1, where $\bar{T} = T - T_{st}$, and

$$c = \phi \left(b_L s_L \sum_k C_L^k \mu^k h_{L,1}^k + b_G s_G \sum_k C_G^k \mu^k h_{G,1}^k \right) + (1 - \phi) H_{CR}. \text{ The main reason is that was noted that}$$

for the much better convergence of the iterative procedure, the pressure-dependent terms, responsible for Joule-Thomson effect and adiabatic heating are worth to be taken out of iteration procedure. Their influence is taken into account after iterations converge. For isothermal flows, the algorithm was repeatedly validated before and demonstrated good convergence and robustness.

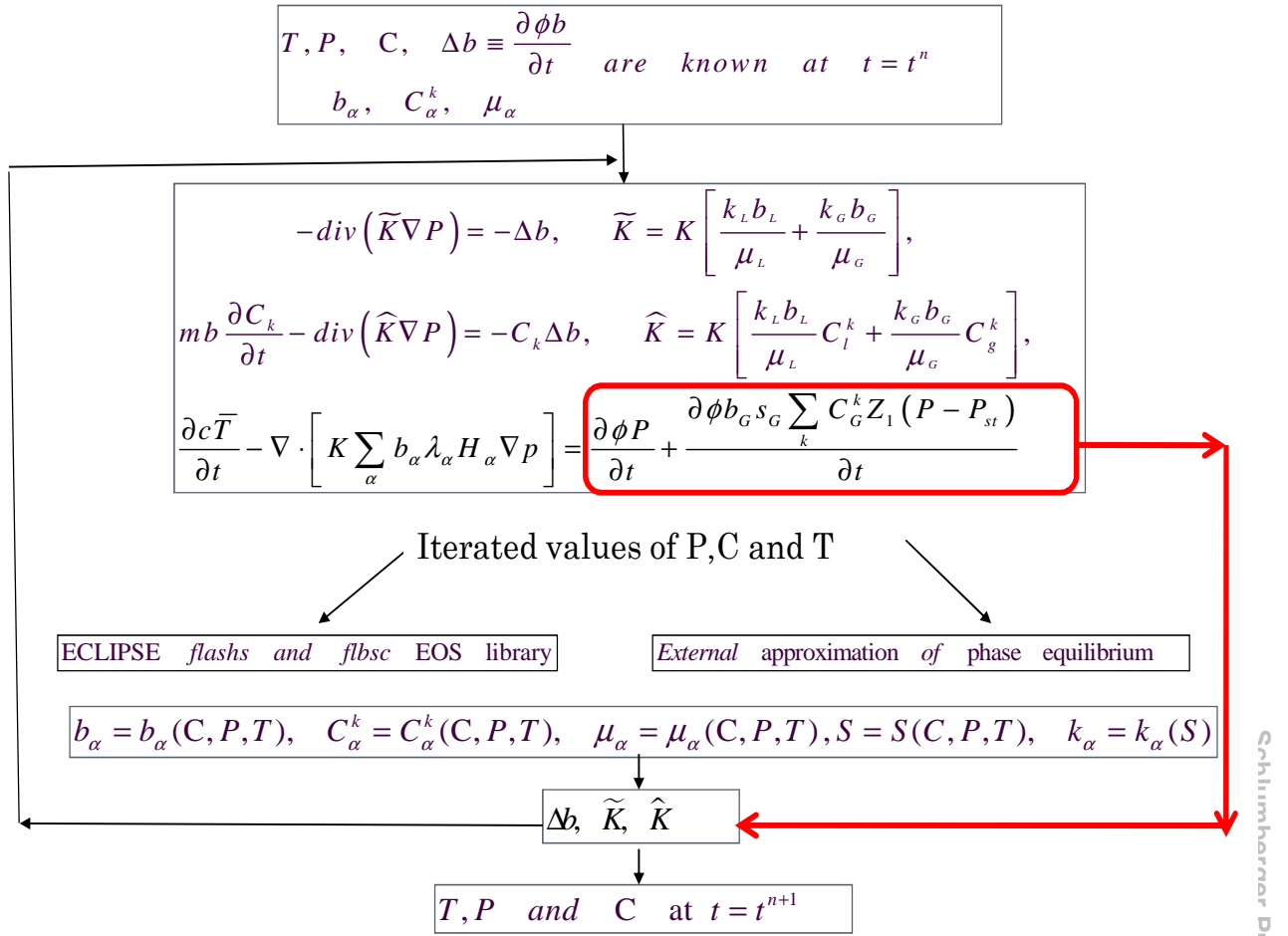


Figure 1. Main steps of algorithm implemented in the thermal compositional research code.

3. E300 Model for the Thermal Option. Validation of the Research Code

To validate newly implemented thermal option we had to choose E300 thermal compositional simulator since nothing more was available for our disposal. However, E300 realization of thermal option for compositional flow hasn't general thermal flash solver, only the version with equilibrium constant being dependent on pressure and temperature is available there. Specifically, after temperature and pressure-dependent K-values K^k are calculated in E300, then phase compositions C_α^k , densities b_α and viscosities μ_α are found by some empirical correlation:

$$C_L^k = \frac{C^k}{1 + (K^k - 1) \cdot S_G}, \quad C_G^k = K^k \cdot C_L^k \quad (9)$$

$$b_L = \frac{1}{\sum_{k=1}^{Nc} C_L^k \frac{\mu^k (1 + C_{T1} \cdot (T - T_{ref})) \cdot (1 - C_p \cdot (P - P_{ref}))}{\rho_{ref}^k}}, \quad b_g = \frac{1}{V_{gas}} = \frac{1}{\sum_{k=1}^{Nc} C_G^k \cdot z^k \cdot R \cdot \frac{T}{P}} \quad (10)$$

Coefficients	E300 keywords	Physical meaning
ρ_{ref}^k	DREF	Oil reference density
T_{ref}	TREF	Oil reference temperature
C_{T1}	THERMEX1	Thermal expansion coefficient
C_p	CREF	Isothermal compressibility

Table 1. Coefficients used in Eclipse for molar density calculations

Then, they are used for further update of primary solution variables.

$$\log(\mu_L) = \sum_{k=1}^{Nc} f_k(C_L^k) \cdot \log(\mu_L^k(T)), \quad \mu_G = \sum_{k=1}^{Nc} C_G^k \cdot \mu_G^k(T) \quad (11)$$

$$f_k(C_L^k) = C_L^k, \quad \mu_L^k(T) = D \cdot T^B, \quad \mu_G^k(T) = A \cdot T^B$$

When values of ZFACT1 are not zero, expression for gas molar volume and, respectively, gas molar density calculations changes:

$$V_G = Z_0^c \cdot \frac{RT}{P} - Z_1^c, \quad b_G = \frac{1}{V_G} \quad (12)$$

These specific correlations were implemented in the research code instead of ‘flash related cell’ in order to check whether the new overall iterative structure related to new thermal terms is correct.

Depending of the problem under consideration, we used at the bound cells pressures and temperatures as given time functions (in particular, constant values). In Table 2 parameters used in calculation are described. Pressure and temperature are fixed on the left and right boundaries. At first, the validating against E300 was performed for the simplified set of gas enthalpy parameters (heat of vaporization at standard temperature was ignored) and with no Joule-Thomson effect.

In Figure 2 it is shown good enough agreement of Research code and Eclipse for non-isothermal calculations. We run these simulation on several grid resolutions and ensures that both codes converges to one and the same result.

Mixture	C1, C4 ,C6
Reservoir Number of cells	2000 m 100, 200, 400, 2000
Permeability Porosity	100 MMD 0.13
Boundary conditions: Pressure (in and out) Temperature (in and out) Concentrations (injected)	80 bars and 40 bars 200°C and 72°C (0.01,0.19,0.8)
Initial data: Temperature Concentrations (reservoir)	72°C (0.89 0.1, 0.1)
SPECHA (kJ/kg/K) SPECHG (kJ/kg/K) HEATVAPS (kJ/kg)	2.21, 1.75, 1.64 2.71 3.0 2.6 830 400 70
HEATCR(kJ/m ³ /K)	74
Time	500 days

Table 2. Parameters used for calculations during validation of research code by comparison with Eclipse.

However, for more complicated gas enthalpy model we stated some disagreement between our simulations and E300.

First, if we introduce in the model for each component non-zero value of heat of vaporization at standard temperature H_0^k (HEATVAPS) we found that the temperature distribution in the E300 solution completely does not depend on the heat of vaporization at standard temperature value for the first component (although it was taken unrealistically huge). We discovered also that when we put this value to zero in the research code and fit the E300 solution then. At the same time, the complete solution of research code is shown in Figure 3 by blue line. The difference is not strong in the case under consideration, but we believe that E300 solution is not correct here since C1 is in the gas phase in the region where we see the difference between the solutions, so it should contribute to the enthalpy.

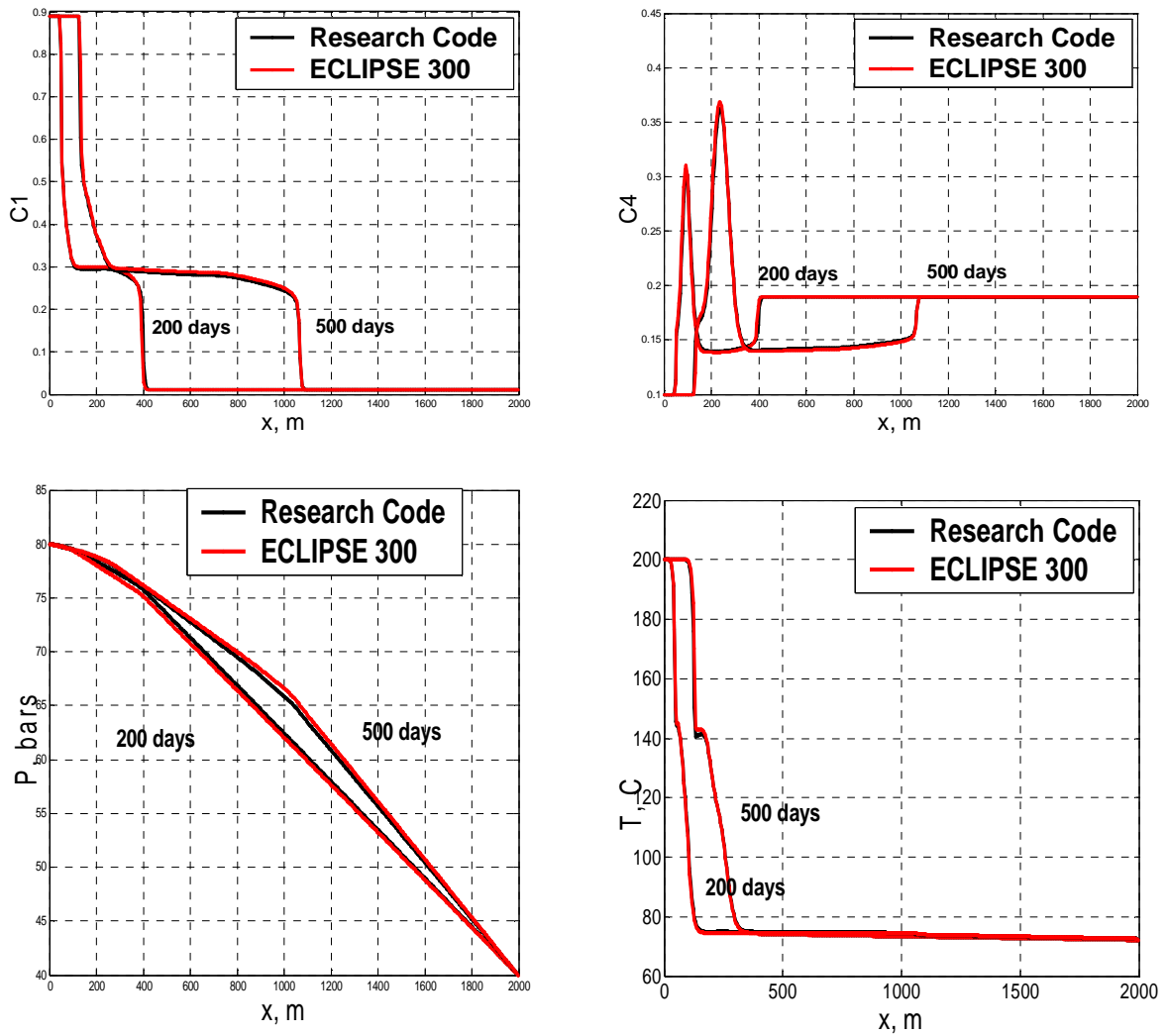


Figure 2. Agreement of Eclipse 300 and research code calculations.

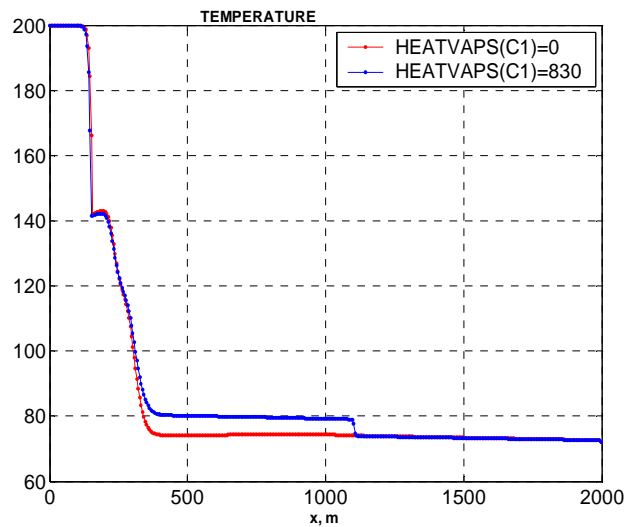


Figure 3. Sensibility of research code calculation results to parameter H_0^k changes

Another discrepancy between our and E300 results occurs when Joule-Thomson effect is taken into account. One can observe non-monotonic dependence of the E300 solution of the Z_1 parameter for which we do not see any physical reason (Figure 4, left). The research code solution is monotonic (Figure 4, right).

We are going to discuss these issues with E300 developers and if they agree with our conclusions and fix the bug we will complete the validation of the code. At the moment we consider our solutions as correct and turn to implementation of external approximations of phase equilibrium.

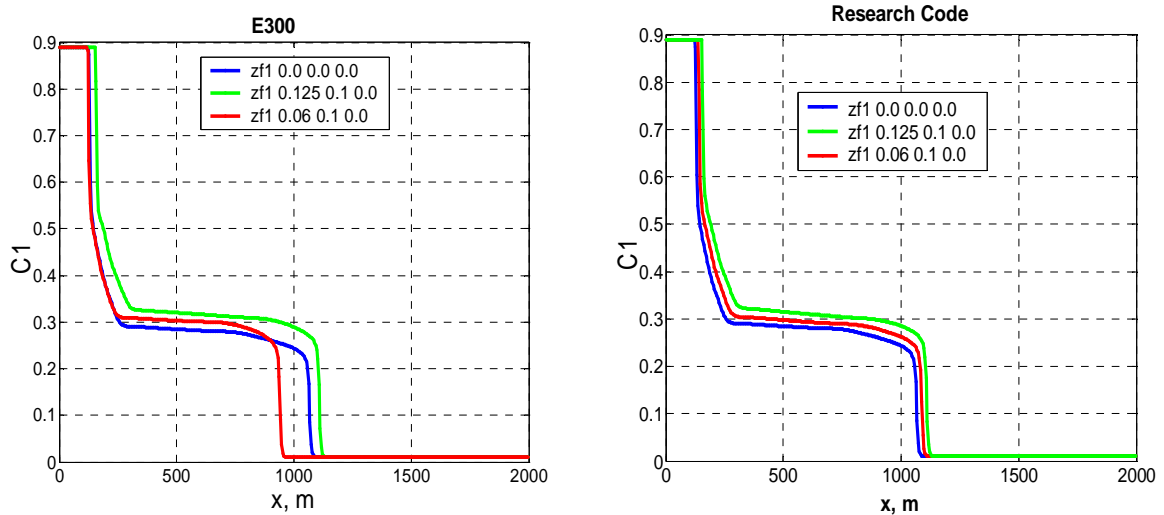


Figure 4. Distribution of C_1 concentration for different Joule-Thomson coefficients

4. Implementation of Temperature Dependent Approximation of Phase Equilibrium Into the Research Code

The approximative technique being developed in SMR for several years is based on the physical fact that in thermodynamic equilibrium there is one-to-one correspondence between bubble points and dew points within a two phase domain. That means, that tie lines (segment across the two phase domain, Figure 5) do not intersect inside it and one can introduce alternative set of independent variables. Namely, for the fixed pressure and temperature each point inside a two phase domain of phase space can be characterized by a scalar ‘leading component concentration’ C_1 and a vector-parameter of tie-lines and $\gamma = \{C_2^m, \dots, C_{N_c-1}^m\}$. The change of the variables from the set $C_1, C_2, \dots, C_{N_c-1}$ to the set C_1, γ has a series of advantages; one of them is that the new set variable is very convenient to perform the precise approximation of phase equilibrium. In the developed in [Belov et al] approximation, so called Q-values

$$Q_k(\gamma) = \frac{C_L^k - C_G^k}{C_L^k + C_G^k} = \frac{1 - K^k}{1 + K^k} \quad (13)$$

are primarily approximated by polynomials in the transcendental way:

$$Q_1^2 = P_1(\vec{\gamma}), \quad Q_k = Q_1 P_k(\vec{\gamma}) \quad (14)$$

The degrees of polynomials can be arbitrary, the higher they are the more precise the approximation is and the more CPU time is expected to reconstruct the phase parameters during hydrodynamic simulations. The simplest case of zero degrees is equivalent to the constant K -values case. Originally, the polynomial approximations were constructed for the fixed P and T . If one need to perform the hydro simulations for the known range of pressure and temperature variations he has to perform the preprocessing work of approximation construction for each P and T in the range, put the polynomial coefficient in a storage and understand a rule how to take them off there during the simulation. In the present job, we extended the previously existent pressure dependent approximation [Levkovich et al.] on the temperature dependent case.

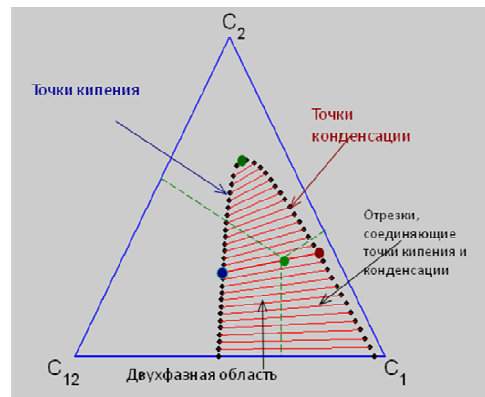


Figure 5. Example of phase diagram for mixture C1C2C12 , P=180 bar, T=200°C.

Implementing the technique into the research code, we first of all insured that if the phase properties are approximated precisely enough, and the number of pressure and temperature splits are large enough, the solution with exact flash and approximations are close enough. For the case presented in Figure 6 the values of the polynomial degrees equal to 2 happen to provide a good accuracy, while 0, that is the constant K -values approximation, is not such good. Then we carried a rapid study on how the temperature split can affect the solution and if it is possible to minimize the number of splits depending on the requested accuracy. The answer is that the number of temperature splits is a decisive factor in non-isothermal flows (Figure 7), and, yes, it is possible to minimize it (Figure 8). However, the low number of temperature split is important for preprocessing work only, so, from a research code point of view that is not an issue.

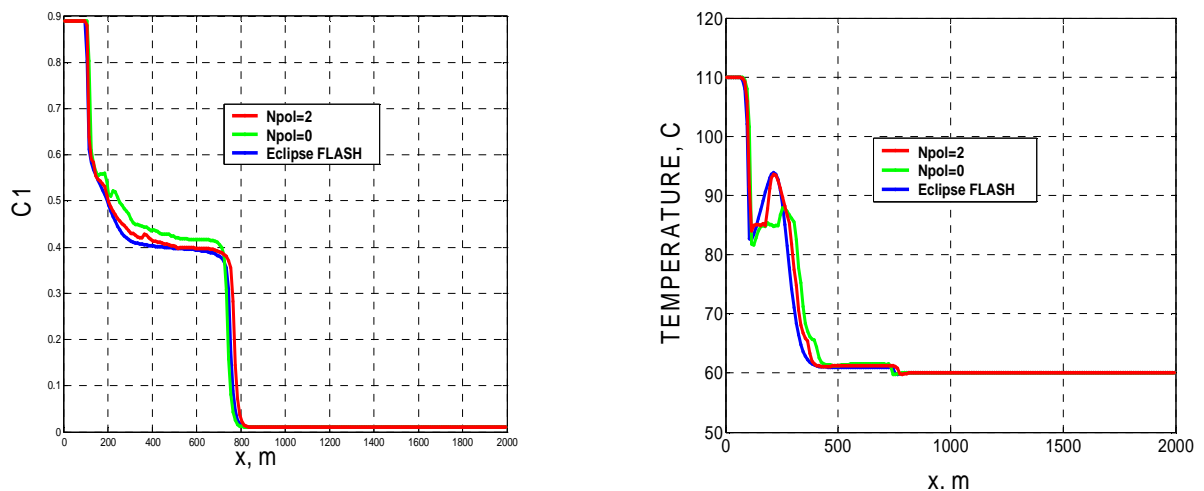


Figure 6. Calculation results with approximations for different polynomial degrees

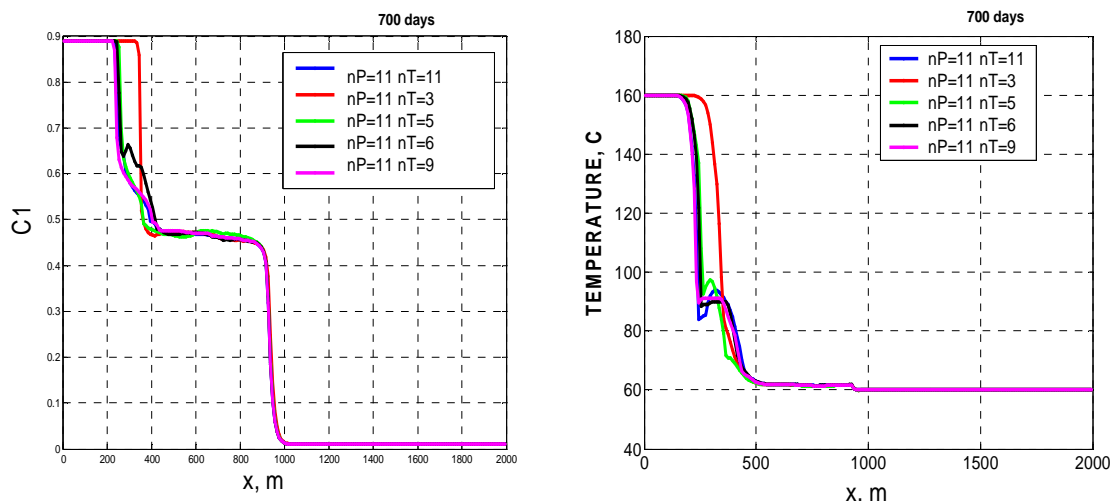


Figure 7. Calculation results with approximations for different temperature splits

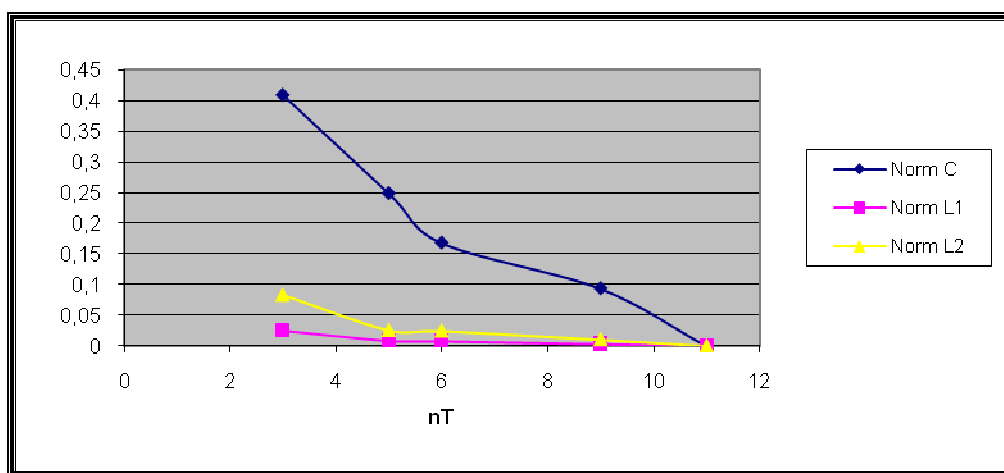


Figure 8. Norms' dependence on number of temperature splits

5. Modeling of Depletion in Gas Condensate Reservoir

We now try to apply the developed technique to the depletion of gas condensate reservoir modeling. It's well known that in gas condensate reservoirs, if condensate bank appears, it can't flow until its saturation is less than specified value:

$$K_{r_0} = \left(\frac{s - s_0}{1 - s_0} \right)^2. \quad (15)$$

Even if it is higher the critical value, it is much less that the mobility of gas, so the bank formation near well bore is not worth. So, if it happens that the bank appeared during depletion, one has to think how to decrease it without decrease of gas recovery. We suggest here to see what will happen if after the bank is formed we start to change borehole pressure in time following some law. So, for the sake of simplicity, let we consider one dimensional flow (Figure 9), with pressure, composition and temperature are kept fixed constant at the outer boundary (chosen such to provide a mixture to be in a gas phase). At the hole, pressure is considered to a

certain function of time, in particular, constant. For the initial temperature, and the expected during depletion pressure, mixture is below dew point at the hole.

The chosen mixture is a model one, just for simple solution of the problem without detail concerns of PVT properties of a real reservoir fluid.

Mixture C1C4C7

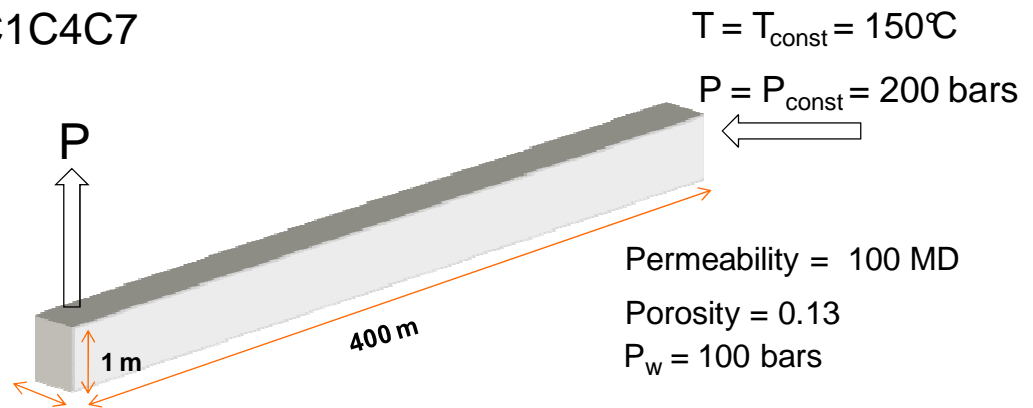


Figure 9. Problem statement for the depletion of a gas condensate mixture

Let us first consider the case $P_h = P_w = const$ and demonstrate the influence of thermal effects of the condensate bank formation. We run thus two simulations with one and same parameters in thermal and isothermal modes. Figure 10 shows overall gas and condensate mass excesses per time, black line corresponds to non-isothermal case, red line – isothermal case. One can see from this picture that condensate bank appears and flow becomes steady during first 40 days. In Figure 11 one color corresponds to same time in all temperature, pressure C1 and condensate saturation distributions. One can see that although the steady-state solutions are quite similar in both cases, the transient flow differs much larger. Namely, for the thermal case the steady state condensate bank is formed later. Also note, that total formation condensate mass is larger in the thermal case. Thus, the first preliminary conclusion is that the neglecting thermal effects in a modeling leads to underestimation of the bank mass in the formation.

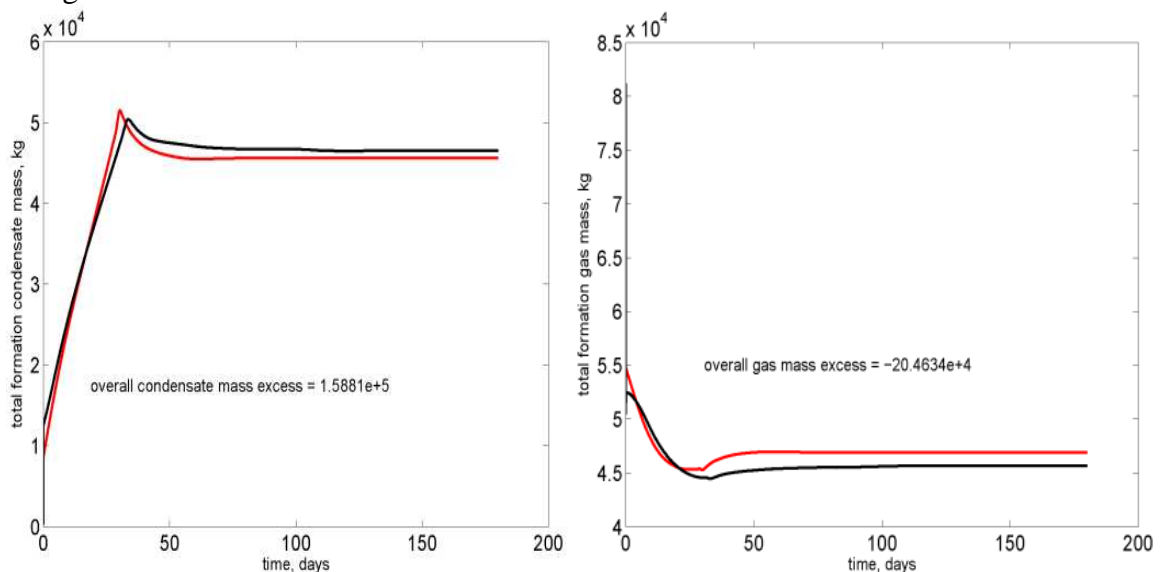


Figure 10. Overall gas (left) and condensate (right) mass excess per time in isothermal (red curves) and non-isothermal (black curves) case

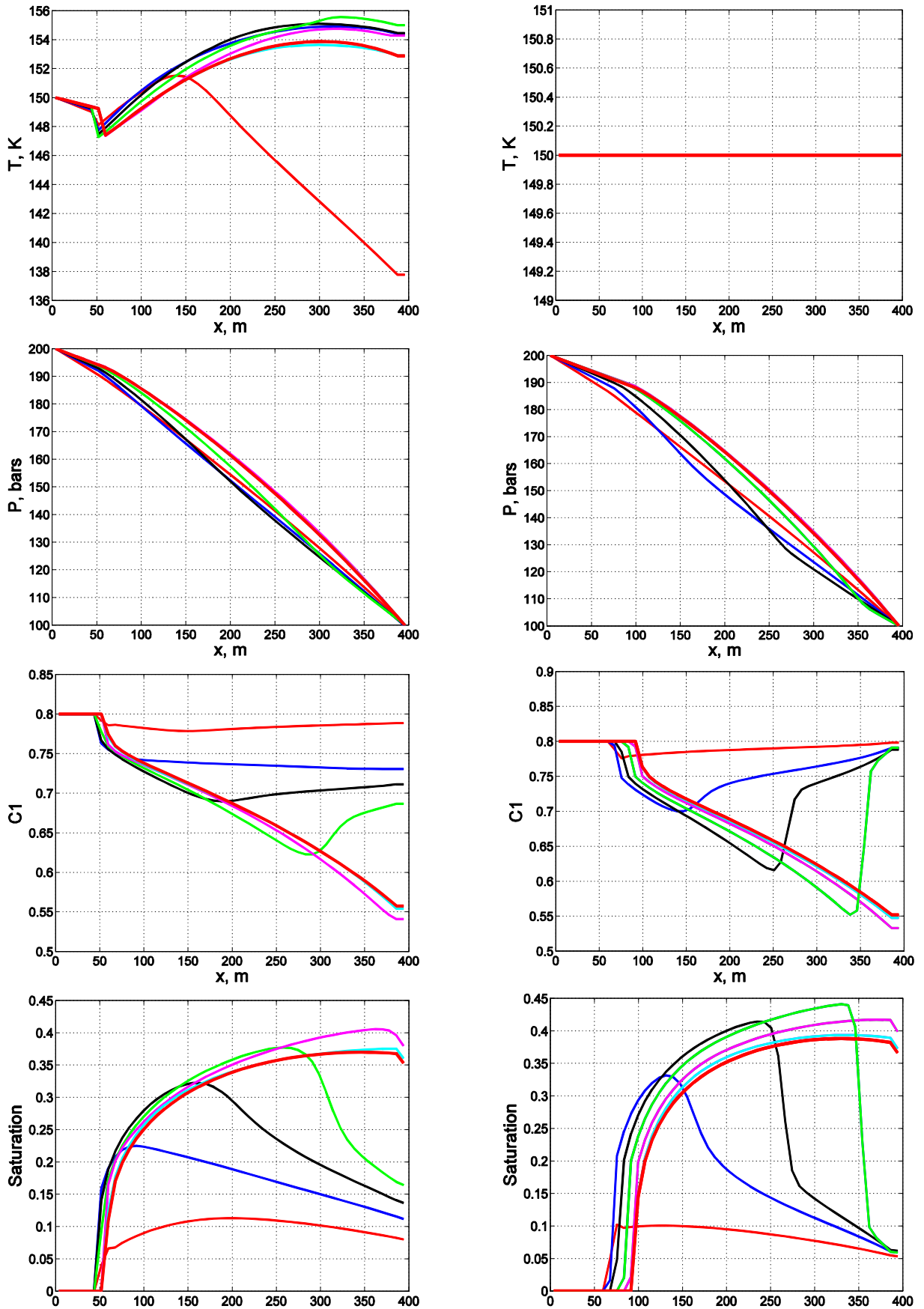


Figure 11. Pressure, C1 concentration and gas saturation distributions for different times (thermal and isothermal cases)

Let us now consider the periodic hole pressure variations according to the law

$$P(t) = \begin{cases} P_w (1 + A \sin^\alpha(\omega(t - t_0))), & t > t_0, \\ P_w, & t \leq t_0 \end{cases} \quad (16)$$

with particular values of parameters $\omega = 0.1 \text{ (days)}^{-1}$, $A = 1/2$, $\alpha = 1$. The value t_0 is taken equal to 60 days to ensure that the flow reaches the stationary regime before the oscillations start.

In Figure 12 one can find different times during fluctuating process illustrated by one and the same color. Also one can see the phase diagrams change in time. In figure 12 those points are marked, phase diagrams have been plotted for: before pressure fluctuations (before formation of condensate bank) – yellow point, under the maximal pressure (red point) and under the minimal pressure (black point).

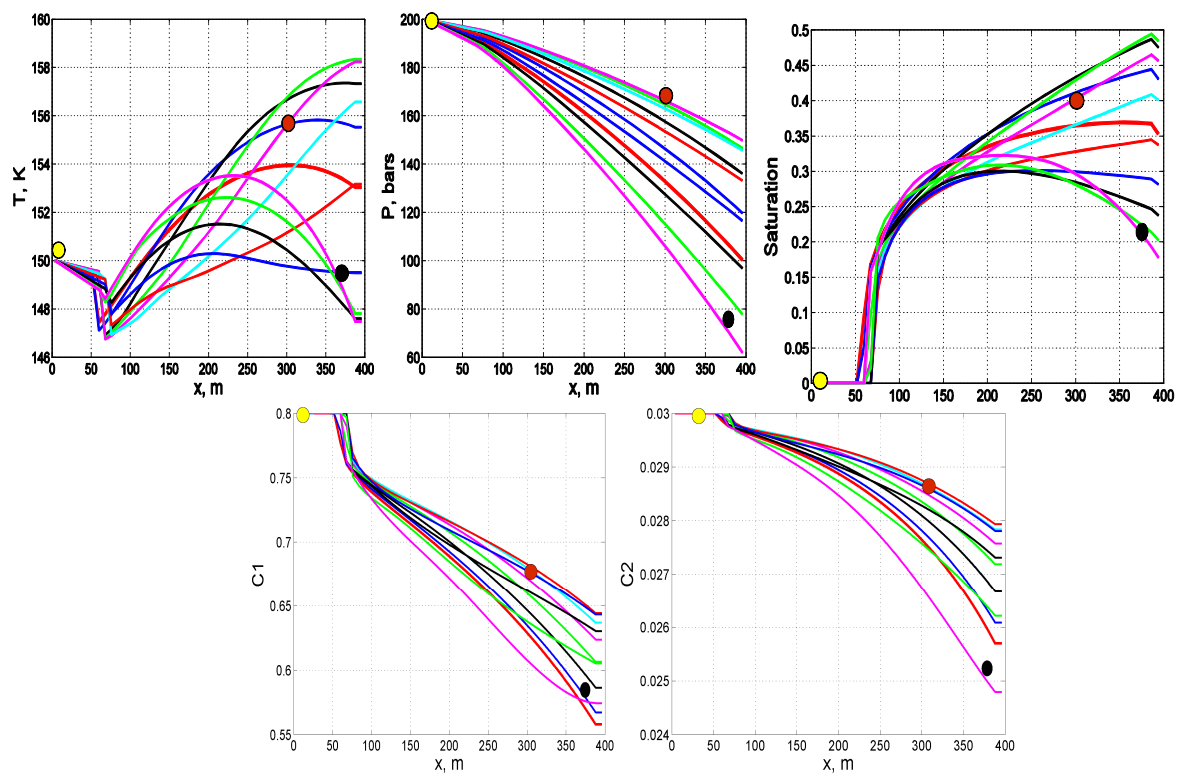


Figure 12. Temperature, pressure, C1 and liquid saturation distributions ad different times

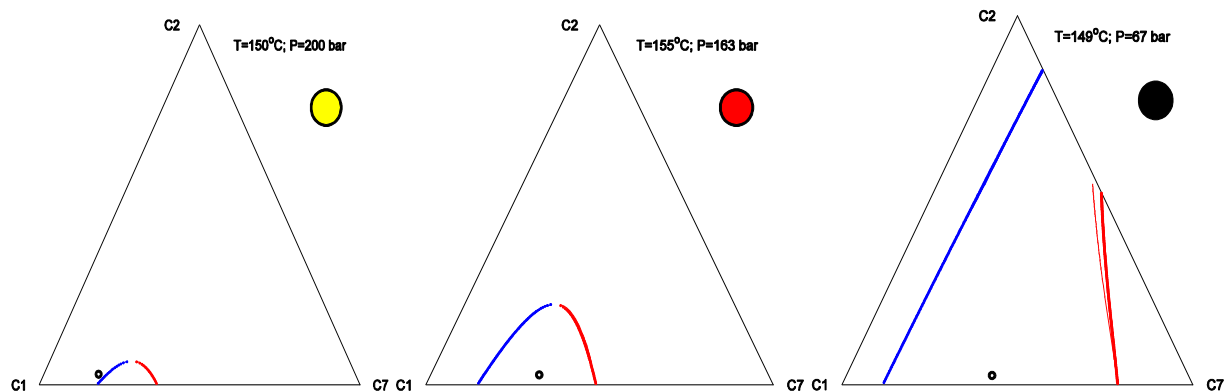


Figure 13. Phase diagrams at different times for different pressures

Phase diagrams in Figure 13 show that, the mixture was in gas phase before pressure fluctuations, and during fluctuating process it was within two phase domain. In this experiment we have a positive influence of pressure fluctuations on the process. In Figure 14 it is shown that overall condensate mass excess is smaller in comparison with one in stationary pressure calculations. It is more illuminating in Figure 15 – cumulative condensate mass excess decreases per time.

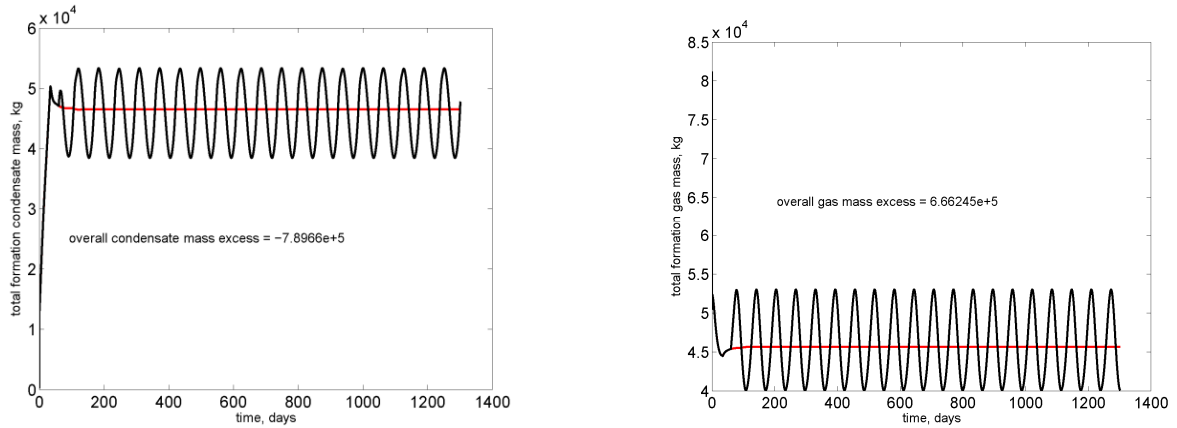


Figure 14. Time dependence of condensate (right) and gas (left) mass during fluctuating (black lines) and steady (red line) pressure regimes

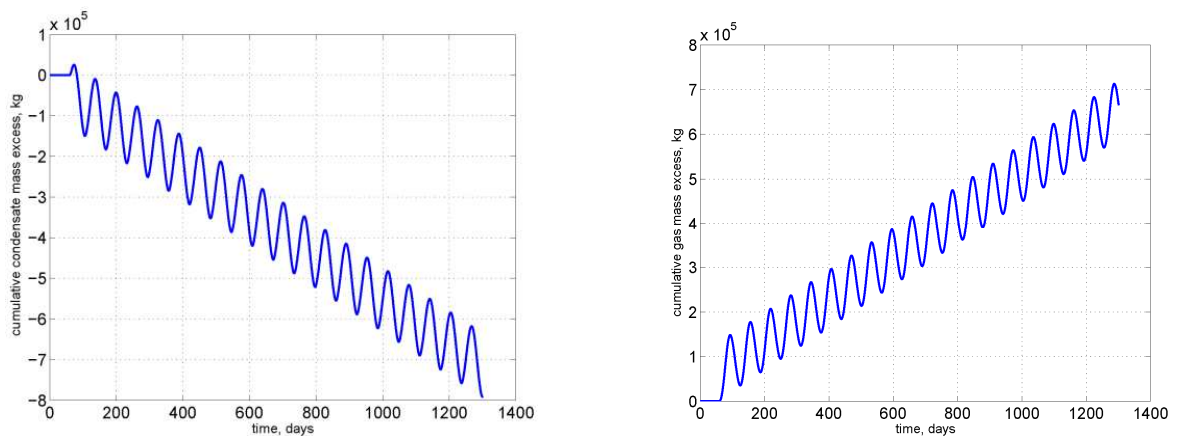


Figure 15. Cumulative condensate (left) and gas (right) mass excess

It was found then that there is dependence between fluctuating regime and overall condensate mass excess. Changes in fluctuating regime change it both for the better and for the worse. The parameters of the calculated cases are presented in Table 3. The corresponding results – in Figure 16 and 17. Note here, that, firstly, oscillation of pressure with one and the same amplitude but with different frequency may lead opposite effect (cases 1 and 2). How to estimate what frequency is ‘good’ and what is ‘bad’ is a challenge and should be discovered for each specific mixture. Secondly, if we change pressure not in oscillating, but in ‘jumping’ mode (cases 3, 4, 5), that is pressure never becomes below initial value, the mass of condensate in reservoir decrease the stronger the larger the amplitude of the jump. However, such regimes obviously decrease gas production, while the oscillating regimes possibly not. It is also worth to be mentioned that absolute values of mass excesses are small (less that 0.1-1 percent, although they growth in time), because we considered just a model mixture consisting only on three light components. We suggest that all these conclusions will take place in experiments with real mixtures.

Table 3. Calculated periodic variants. Colored line in the first column correspond to the line in Figure 16. Number in the last column – to the panel number in Figure 17

Lines in Figure 16	ω	A	α	Panels in Figure 17
—	1	0.5	1	(1)
—	0.1	0.5	1	(2)
—	0.1	-0.5	2	(3)
—	0.1	1/Pw	2	(4)
—	0.1	0.5	2	(5)

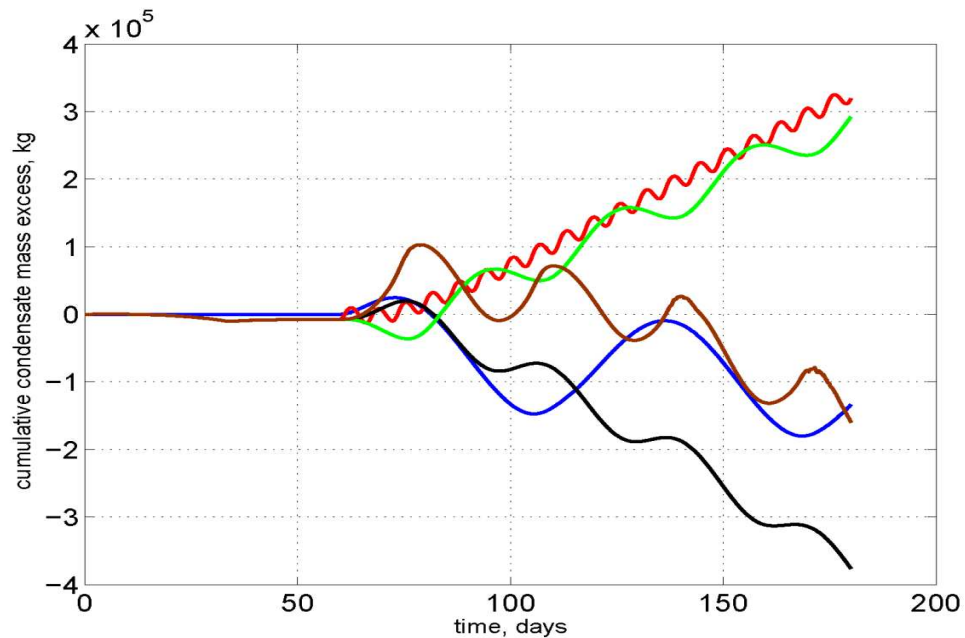


Figure 16. Cumulative condensate mass excess for various regimes presented in Table 3

6. Conclusions

- Development and validation of thermal composition General Purpose Research Code was done. In general, the coincidence with the E300 is perfect, but in some discrepancy with E300 are found out, and the results of the research code look more physical reliable. The discrepancy has to be discussed with the E300 developers.
- The preprocessing phase approximation developed previously on the isothermal case is extended into non-isothermal calculations
- In the gas condensate depletion modeling we found: firstly, that neglecting of thermal effects lead to underestimation of gas condensate bank mass in reservoir; secondly, that borehole pressure change after the bank is formed may lead both to positive and negative effects. This result is nontrivial and needs further investigations.

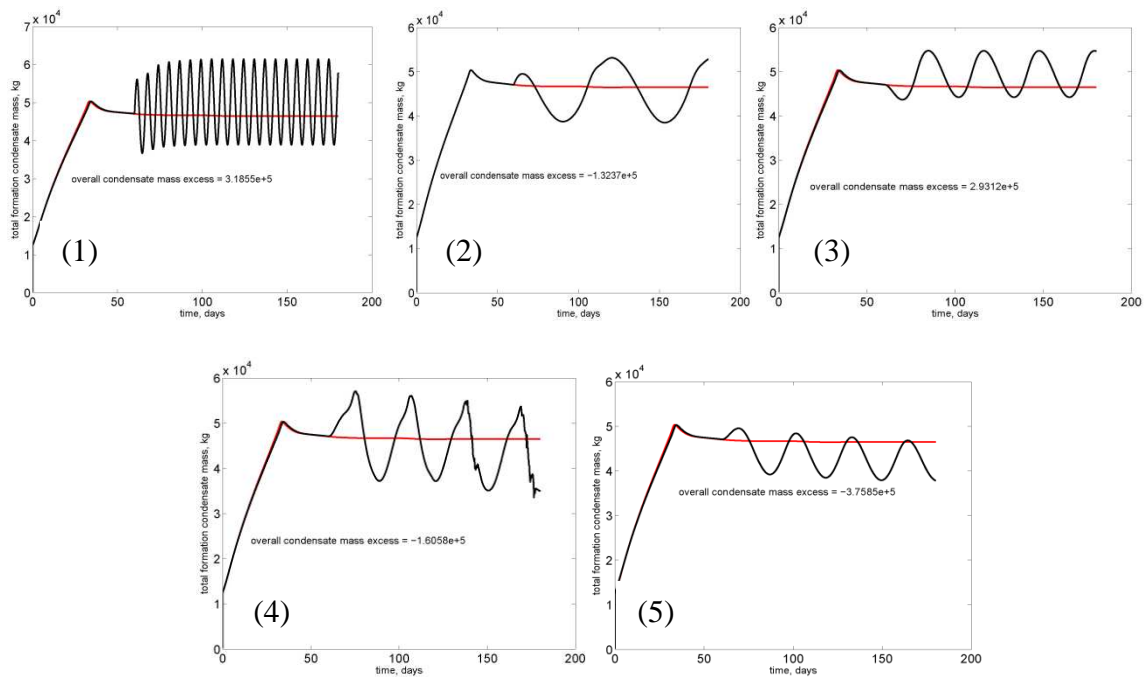


Figure 17. Time dependence of condensate mass for the cases presented in Table 3

7. References

[Belov et al]: Belov N., A. Myasnikov, K. Bratvedt, “Precise Approximations of Phase Equilibrium of Multicomponent Hydrocarbon Mixtures”, OFSR/RN/2008/068/SMRMM/C

[Levkovich et al]: Levkovich-Masluk L., V. Lysov, Yu. Rykov, A. Myasnikov, K. Bratvedt, “Fast Compositional Solver in Streamline-Based Reservoir Simulations: Constant K-value Approximations”, OFSR/RN/2008/070/SMRMM/C

[Lysov et al]: Lysov V., O. Podgornova, Yu. Rykov, A. Myasnikov, K. Bratvedt, “Fast Approximation of Phase Equilibrium Based on Random Sampling and its Application for Compositional Streamline Simulations”, OFSR/RN/2008/071/SMRMM/C